J Mater Sci: Mater Electron (2023) 34:1090

Effect of sintering temperature on properties of Ba ($Cu_{1/2}W_{1/2}$) O_3 high dielectric ceramics

Juanjuan Wang[1,*], Bochao Xie[1], and Xueliang Duan[1]

[1] School of Materials Science and Engineering, Xi'an University of Technology, Xi'an 710048, Shaanxi, China

Received: 20 March 2023
Accepted: 17 April 2023
Published online: 4 May 2023

ABSTRACT

Ba ($Cu_{1/2}W_{1/2}$) O_3 (BCW) ceramics were prepared and their dielectric properties were investigated for energy storage applications. A low pre-sintering temperature of 930 °C was used to achieve favorable grain crystallinity, and a sintering temperature of 1160 °C was used to obtain a high dielectric constant. A dielectric constant of 10^5 was observed at 10 Hz and 400 °C. Moreover, the BCW ceramics exhibited good microstructure and optimal temperature stability over a wide temperature range from − 100 to 500 °C, and the internal barrier layer capacitance mechanism was considered to be the reason for their high dielectric performance. The surfactant PEG was found to be the most effective in enhancing the dielectric properties of BCW ceramics. This study demonstrates the potential of this material for high-density energy storage applications.

1 Introduction

With the increasing demand for microelectronic devices such as capacitors, resonators, and filters, researchers are searching for new materials with high dielectric constants, with a dielectric constant as high as 10^3 [1–4]. Various high dielectric constant materials have been reported in the literature, including typical perovskite ferroelectric materials, composite cubic perovskite-like oxide $ACu_3Ti_4O_{12}$ with an internal barrier layer capacitor (IBLC) effect, and TiO_2 dipole ceramics with electron fixed defect dipoles [5, 6]. Unfortunately, due to weak d_{33}, most of these materials are not suitable for commercial use in high-density storage applications [7–11]. The objective of this study is to obtain tungsten copper barium acid (BCW) ceramic materials with high dielectric constant (ε) and low dielectric loss (tan δ), using a solid-phase sol–gel two-step method to prepare tungsten copper barium acid $Ba(Cu_{1/2}W_{1/2})O_3$ ceramics, and analyze the relationship between size effects and properties. The solid-phase sol–gel two-step process is a superior approach for preparing BWC ceramics, offering better uniformity, control over material properties, and low-temperature preparation [12]. This method yields ceramics with high density, mechanical strength, and excellent dielectric properties [13]. In this article, we studied the effects of different surfactants on ceramic properties compared the effects of different surfactants on ceramic dielectric properties and compactness, and adjusted the pH value to optimize the system. We also explored the pre-sintering temperature and sintering temperature, as well as the effects of different

Address correspondence to E-mail: juanwang@xaut.edu.cn

https://doi.org/10.1007/s10854-023-10484-w

sintering temperatures on the size and properties of tungsten copper barium acid ceramics.

2 Experimental procedures

Ba ($Cu_{1/2}W_{1/2}$) O_3 ceramic was synthesized using solid-phase sol–gel two-step process approach with $BaCO_3$, CuO, and WO_3 as starting materials, weighted according to stoichiometric composition. The beaker containing the solution was placed in an oil bath set at 80 °C for three minutes. Then, ammonia solution was added to adjust the pH of the solution to 6.5, and water was added to the desired volume. The system was then allowed to react and form a sol in the oil bath. The resulting sol was removed from the oil bath and aged at room temperature for 12 h to form a gel, which was then dried at 120 °C for 24 h to obtain the dried gel of barium copper tungstate. The dried gel was ground to form a convenient powder which was then placed in a crucible and pre-sintering at 950 °C for 5 h to form a ceramic precursor powder. Polyvinyl alcohol (5 wt.% PVA) was added to the pre-sintering BCW powder as a binder, followed by granulation and sieving. The powder was then pressed into pellets (6 MPa pressure) with each pellet weighing 0.4 g. After pressing, the pellets were degassed at 500 °C for 3 h and sintered at 1160 °C for 6 h to obtain the final ceramic sample. Silver electrodes were deposited on both surfaces of the sample by sputtering at 850 °C for 30 min. The main steps of the experiment are shown in Fig. 1.

The phase structure was characterized by x-ray diffraction (XRD, D/max-2550, Rigaku, Japan, Cu-K_α, Ni filter, k = 1.5418 Å) in the 2 h range of 30° to 80° in steps of 0.02 at room temperature and 40 kV /30 mA. The surface microstructure was checked by scanning electron microscopy (SEM, model Quanta 200, FEI Company, Eindhoven, The Netherlands). The complex impedance was measured by using an Agilent 4294A (Palo Alto, CA) impedance analyzer.

3 Results and discussion

The XRD pattern of the BCW powder is shown in Fig. 2. All major diffraction peaks in the XRD pattern could be indexed to Joint Committee on Powder Diffraction Standards (JCPDS) card no. 38–1378 with no secondary phases detected, indicating that a single BCW phase was obtained after calcination at 930 °C and 950 °C for 5 h.

The peak of the main crystalline phase is also sharpest when the sintering temperature is 930 °C. By analyzing the XRD spectra of BCW ceramic pre-sintering powders at different pre-sintering temperatures, we demonstrated that the choice of 930 °C was suitable, which is conducive to the improvement of the denseness of the Barium Tungsten-Copperate ceramic materials.

Figure 3 shows the SEM image of the BCW sample sintering temperatures at 1060 °C, 1160 °C, 1190 °C. It was found that the grain size of BCW ceramics becomes larger with the increase of sintering temperature from the SEM images. As the sintering temperature of BCW ceramics increased, the crystallization rate accelerated and the crystal growth became more sufficient, which led to recrystallization and grain-boundary migration. These processes could cause an increase in grain size. In addition, high-temperature sintering could also cause defects and oxide migration within the crystals, further promoting grain growth [14–19]. We found that the optimal grain size image was obtained at a pre-sintering temperature of 1160 °C. Furthermore, with an increase of the sintering temperature, the surface porosity of the barium tungstate ceramic decreased and the denseness of the BCW ceramic became greater. This is supported by the density variation of

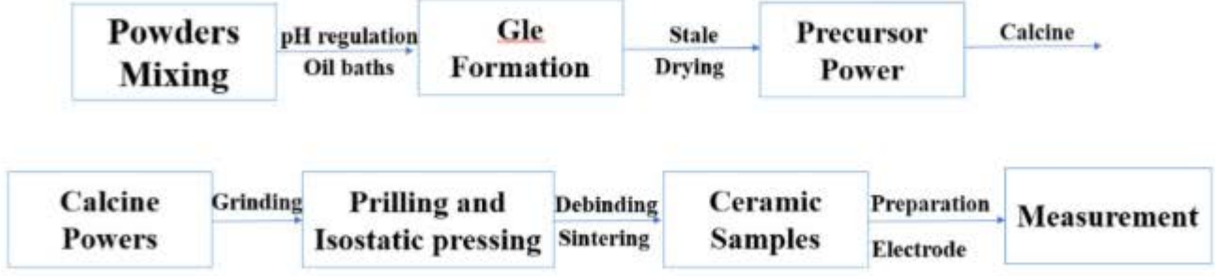

Fig. 1 The main steps of solid-phase sol–gel two-step process

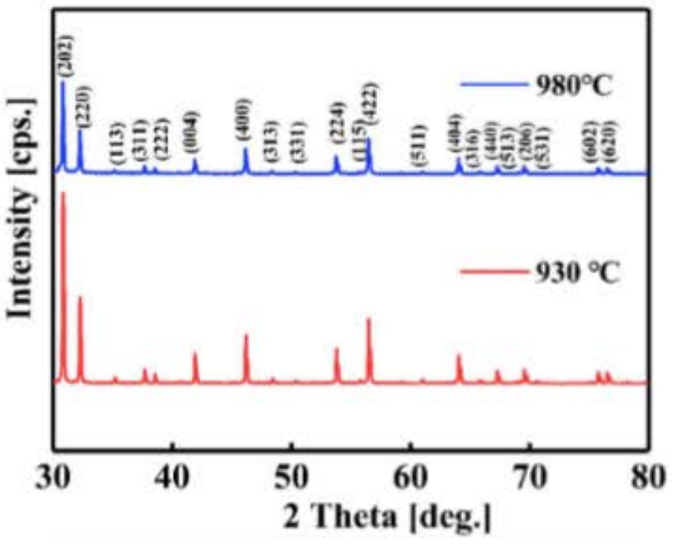

Fig. 2 XRD spectrum of barium tungsten copperate ceramic powders with different pre-sintering temperatures

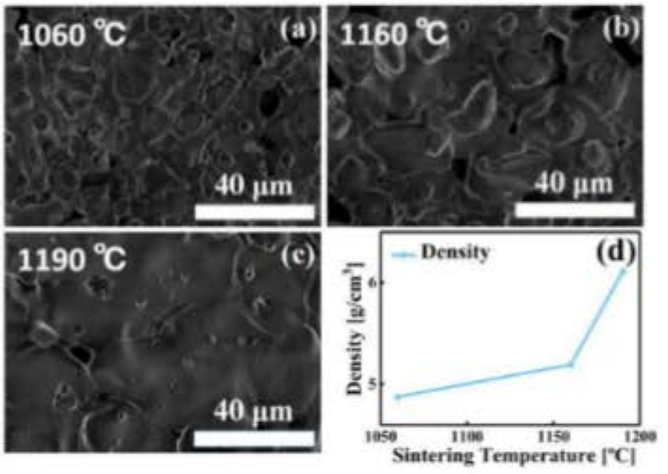

Fig. 3 **a**–**c** SEM images of BCW ceramics with different sintering temperatures **d** Density variation of BCW ceramics with different sintering temperatures

BCW ceramics at different sintering temperatures shown in Fig. 3d: the density of BCW ceramics increases with increasing sintering temperature. The density exhibits a slow increase before the sintering temperature reaches 1160 °C, followed by a rapid increase thereafter. The higher the sintering temperature, the denser the BCW ceramic.

The grain size distribution and aspect ratio of BCW ceramics sintered at temperatures of 1060 °C, 1160 °C, and 1190 °C are shown in Fig. 4. It can be observed that as the sintering temperature increases, the crystal size increases, and the span of the overall crystal size decreases. From Fig. 4a, it can be seen that in ceramics sintered at 1060 °C, a large proportion of grain sizes are located in the range of 12–15 μm; for ceramics sintered at 1160 °C from Fig. 4b, grain sizes are in the range of 20–30 μm; and for ceramics sintered at 1190 °C from Fig. 4c, grain sizes are concentrated around 50 μm. The increasing proportion of larger grain sizes demonstrates the consistency of the grain size distribution. Finally, from Fig. 4d we conclude that there is a relationship between the average grain size (AGS) and the sintering temperature. Before 1160 °C, the AGS increases slowly in a linear manner with the sintering temperature, followed by a faster linear increase.

Figure 5a, b shows the frequency dependence of the dielectric constant and dielectric loss of BWC ceramics at different temperatures. According to Fig. 5a, the dielectric constant decreases as the frequency increases. At low frequencies, an electric field induces molecular or ionic motion in a material, which can greatly increase the dielectric constant. However, at high frequencies, the electric field changes rapidly in a very short period, which does not provide enough time for molecules or ions to follow the field and move, thus reducing the dielectric constant. This frequency dependent response of the dielectric constant is due to the different interaction mechanisms between molecules or ions and the electric field at different frequencies [20, 21]. As shown in Fig. 5b, two dielectric loss peaks observed at 0 Hz and at about 10^6 kHz for the BCW ceramic. The high-frequency dielectric loss peak was weakened, corresponding to the depressed intensity of the dielectric relaxation in Fig. 5a. At low frequencies, the dissipative mechanisms such as ionic motion and molecular rotation induced by an electric field are significant, leading to an increase in dielectric loss with increasing temperature. In contrast, at high frequencies, the rapid change of the electric field does not provide sufficient time for the internal molecules or ions to respond to the field, resulting in a decrease in dielectric loss with increasing temperature. Additionally, at high temperatures, the molecules or ions inside the dielectric are more likely to undergo ionization, which lowers the loss factor of the dielectric and ultimately reduces the dielectric loss with increasing frequency. The dielectric loss of the BCW ceramic decreases with frequency at all temperatures as shown in Fig. 5b. The optimal sintering temperature for the barium copper tungstate (BCW) ceramic material was determined to be 1160 °C based on the observed highest dielectric performance at this

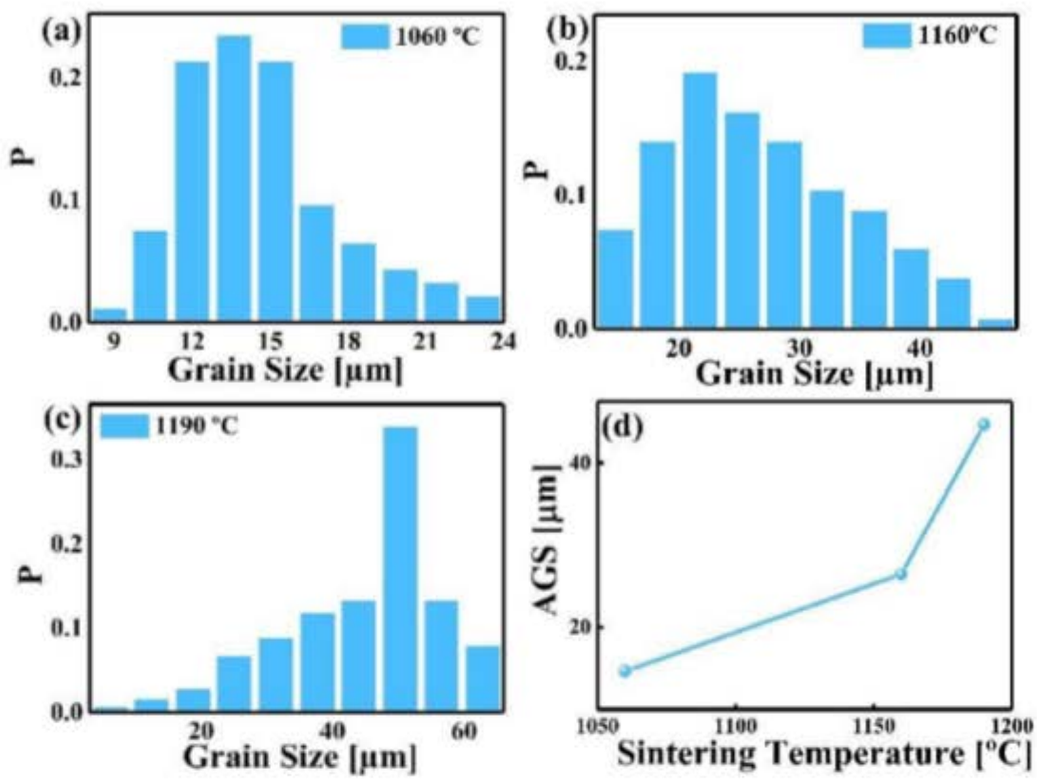

Fig. 4 Variation of size of BCW ceramics at different sintering temperatures **a** 1060 °C **b** 1160 °C **c** 1190 °C **d** Folding line graph of average grain size variation

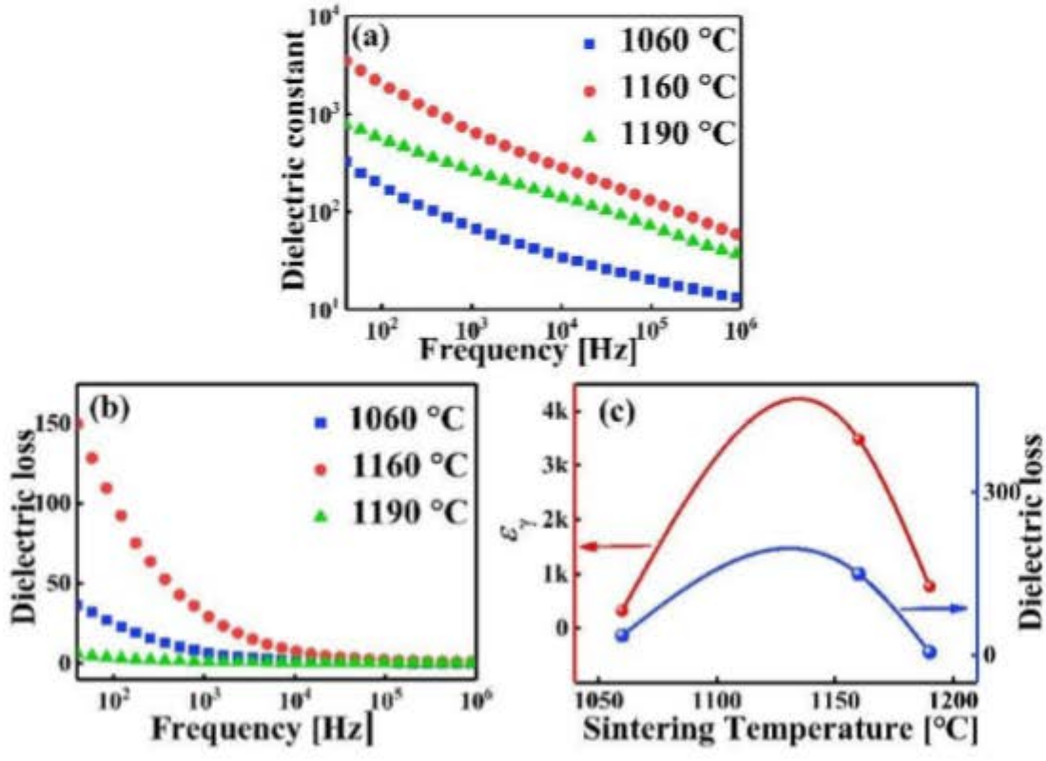

Fig. 5 Dielectric spectrum of room temperature barium tungsten copperate ceramic **a** Variation of dielectric constant **b** Variation of dielectric loss **c** Dielectric spectrum at 40 Hz

temperature, while the dielectric performance was relatively lower at 1190 °C. The dielectric performance of the BCW ceramic material initially increased and then decreased with increasing sintering temperature, as shown in Fig. 5c. These results suggest that the sintering temperature has a significant impact on the dielectric properties of BCW ceramics.

Figure 6 presents the temperature-frequency dependent dielectric constant and dielectric loss of BCW ceramics sintered at 1160 °C at low temperatures. Observational analysis revealed that the

dielectric constant of BCW ceramics increases with increasing temperature, reaching a maximum peak at 200 °C, and has its lowest value at temperatures below − 100 °C. Additionally, the dielectric constant decreases with increasing frequency, with a maximum value of 10^4 at 0.1 kHz and 200 °C. The dielectric loss at different frequencies exhibits an increasing trend with increasing temperature, but the rate of increase varies with frequency. The lower the frequency, the faster the dielectric loss increases with temperature. At 0.1 kHz, a dielectric loss of 8 or more can be achieved at around − 100 °C, whereas for frequencies above 100 Hz, temperatures of 200 °C or higher are required. These findings suggest that BCW ceramics have promising potential for use in high-temperature applications.

Figure 7 presents the temperature-frequency dependent dielectric constant and dielectric loss of BCW ceramics sintered at 1160 °C at high temperatures. From Fig. 7a, that the dielectric constant increases with temperature before 270 °C. By observing Fig. 7b, it can be seen that the dielectric loss is almost 0 in this temperature range. However, in the temperature range of 270–500 °C, the dielectric loss exhibits a rapid increase due to the distribution state transition of oxygen vacancies from static to dynamic disorder, resulting in a dielectric anomaly. In general, in the Dielectric Loss-T plot shown in brown in Fig. 7b, a Debye-like relaxation is accompanied by the appearance of a dielectric loss peak. As shown in Fig. 7b, a dielectric loss peak can be observed in BCW ceramics at around 250 °C. It can be seen that the low-temperature dielectric loss peak corresponding to Fig. 7a is weakened, corresponding to the suppression intensity of dielectric relaxation shown in Fig. 7a. The disappearance of the high-temperature dielectric loss peak may be due to the higher conductivity at high temperatures, which may mask the expected dielectric loss peak.

Figure 8 presents the temperature-dependent dielectric performance spectrum of BCW ceramics sintered at 1160 °C, where Fig. 8a and b demonstrate that the dielectric properties and dielectric loss of BCW ceramics decrease with increasing frequency, while their dielectric constants and losses increase with increasing temperature. Moreover, it can be observed from Fig. 8b that the dielectric loss almost reaches 0 at a frequency of 10^5. Figure Fig. 8c displays the temperature-dependent complex impedance spectrum of the BCW ceramic. Generally, impedance spectroscopy analysis is a better approach to reveal the mechanisms underlying dielectric properties. At different temperatures, only a semicircular arc was observed, gradually evolving with increasing temperature. The semicircular arc at low temperature is attributed to contributions from grain boundaries, while the arc at high temperature is attributed to the contributions of grains. From Fig. 8c, it can be inferred that the influence of grain boundaries on the conductivity of BCW ceramics decreases with increasing temperature.

All the diffraction peaks occurring on the XRD patterns of the barium tungsten copperate ceramic flakes with the addition of the three surfactants are consistent with the powder diffraction standard card (JCPDS No. 38–1378) as seen in Fig. 9, which indicates that the addition of all three surfactants leads to a single BCW phase. Research has shown that PEG can increase viscosity, prevent solid particle aggregation, and thereby enhance homogeneity and stability during ceramic preparation. Citric acid, an organic acid, can react with ceramic surface oxides to form soluble complexes that enhance adhesion and stability, and improve corrosion resistance [22, 23].

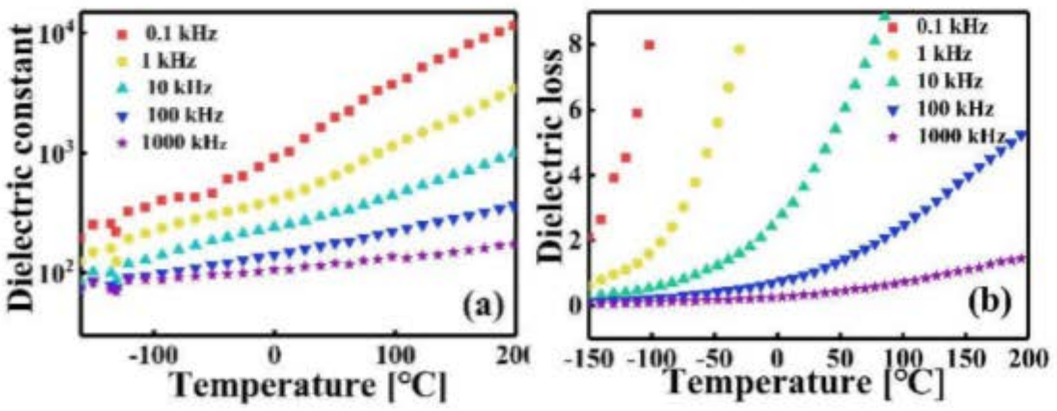

Fig. 6 Low temperature dielectric properties of barium tungsten copperate ceramics sintered at 1160 °C: 0.1, 1, 10, 100 and 1000 kHz **a** Dielectric properties **b** Dielectric loss

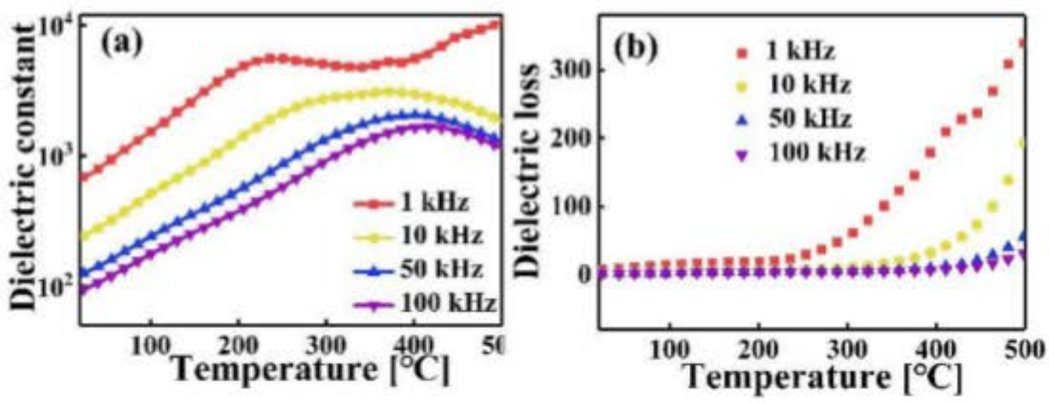

Fig. 7 High temperature dielectric properties of barium tungsten copperate ceramics sintered at 1160 °C: 1, 10, 50, 100 kHz **a** Dielectric properties **b** Dielectric loss

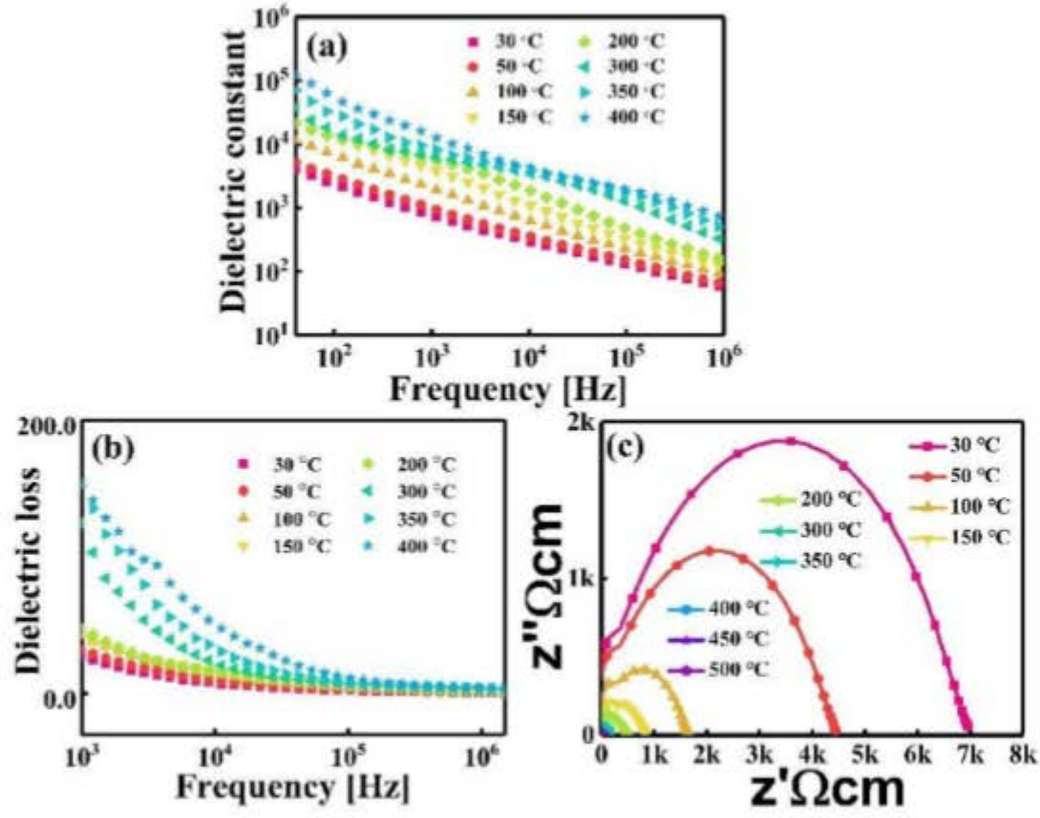

Fig. 8 Variable temperature dielectric properties of barium tungsten copperate ceramics sintered at 1160 °C: 30, 50, 100, 150, 200, 300, 350, 400 °C **a** Dielectric properties **b** Dielectric loss **c** Impedance: 30, 50, 100, 150, 200, 300, 350, 400,450,500 °C

Simultaneously adding PEG and citric acid can further improve these properties, increasing homogeneity, stability, corrosion resistance, adhesion, and reliability of ceramics.

4 Conclusions

A novel colossal-permittivity Ba $(Cu_{1/2}W_{1/2})O_3$ ceramic was successfully prepared by the solid-phase sol–gel two-step process and their properties were analyzed at different sintering temperatures. The optimum dielectric performance of BWC ceramic was achieved at a pre-sintering temperature of 930 °C and a sintering temperature of 1160 °C. The dielectric behavior of the ceramic was investigated at different temperatures and frequencies, revealing a very high dielectric constant of 10^5 at 400 °C and 10 Hz. Furthermore, Peg was identified as the most effective surface active agent for improving the dielectric properties of the ceramic. By analyzing the electrical impedance results and applying the Arrhenius law, it can be inferred that the giant permittivity observed in the BCW ceramic is a result of the internal barrier layer capacitance effect [24]. Moreover, the ceramic showed two distinct dielectric constant plateaus at low and high temperatures, which can be attributed

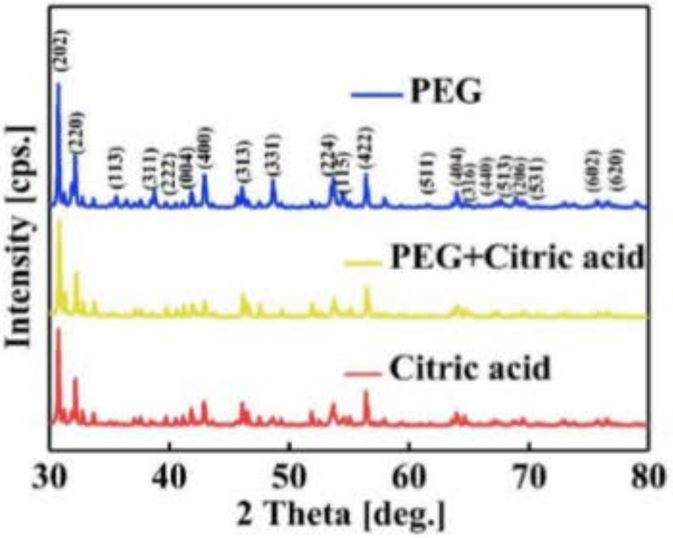

Fig. 9 XRD images of BCW ceramics with different surfactants

to the grain and grain-boundary responses, respectively.

Author contributions

JW and BX: contributed to the conception and design of study. JW, BX, and XD: The materials preparation and data collection were performed. JW and BX The analysis and interpretation of data were done. BX and XD: The first draft of the manuscript were completed. JW: revised the manuscript critically for important intellectual content. All authors reviewed and approved the final manuscript.

Funding

The authors gratefully acknowledge the funding of National Nature Science Foundation of China (NSFC, 51174160) and Natural Science Foundation of Shaanxi Province in China (101–221206).

Date availability

The authors confirm that the data supporting the findings of this study are available within the article.

Declarations

Conflict of interest The authors declare that they have no known competing financial interests or personal relationships that could have appeared to influence the work reported in this paper.

Ethical approval The authors declare that there is no ethics problems.

Research data policy These policies make it easier for researchers to share data and files that support their publications and improve author service and experience.

References

1. H.B. Yang, L.Y. Bai, Y. Lin, F. Wang, T. Wang, Ceram. Int. **43**, 2903–2909 (2017)
2. T.L. Yu, Z. Zhao, J.C. Li, Ceram. Int. **47**, 9948–9955 (2022)
3. S. Peng, Y. Zhang, J.J. Tang, W.F. Zeng, C.L. Zhao, J. Mater. Sci.: Mater. Electron. **32**, 23309–23316 (2021)
4. Y.W. Chen, M.R. Zhang, H.Y. Yang, E.Z. Li, Ceram. Int. **48**, 12118–12125 (2022)
5. F. Li, W. Cui, Y. Shao, J. Zhang, S.M. Du, Z.L. Chen, Z.B. Tian, K.X. Chen, G.H. Liu, Mater. Chem. Phys. **287**, 126365 (2022)
6. H. Li, P.C. Zhang, S.Q. Yu, H.Y. Yang, B. Tang, F.H. Li, S.R. Zhang, Ceram. Int. **45**, 11639–11647 (2019)
7. P.Y. Zhao, Z.M. Cai, L.L. Chen, L.W. Wu, Y. Huan, L.M. Guo, L.T. Li, H. Wang, X.H. Wang, Energy Environ. Sci. **13**, 4882–4890 (2020)
8. H. Palneedi, M. Peddigari, G.T. Hwang, D.Y. Jeong, J.H. Ryu, Adv. Funct. Mater. **28**, 1803665 (2018)
9. D.X. Li, X.J. Zeng, Z.P. Li, Z.Y. Shen, H. Hao, W.Q. Luo, X.C. Wang, F.S. Song, Z.M. Wang, Y.M. Li, J. Adv. Ceram. **10**, 675–703 (2021)
10. J.L. Li, Z.H. Shen, X.H. Chen, S. Yang, W.L. Zhou, M.W. Wang, L.H. Wang, Q.W. Kou, Y.C. Liu, Q. Li, Z. Xu, Y.F. Chang, S.J. Zhang, F. Li, Nat. Mater. **19**, 999–1005 (2020)
11. F.E. Bouharras, M. Raihane, B. Ameduri, Prog. Mater. Sci. **113**, 100670 (2020)
12. R. Xiang, H. Li, P.C. Zhang, X.Q. Chen, H.L. Hu, Q.Z. Wen, S.C. Liu, Ceram. Int. **47**, 8447–8452 (2021)
13. M.K. Du, L.X. Li, L.Z. Ni, Y. Zhan, Ceram. Int. **47**, 19716–19726 (2021)
14. K. Surendran, M. Sebastian, P. Mohanan, R. Moreira, A. Dias, Chem. Mater. **17**, 142–151 (2004)
15. P.F. Ning, L.X. Li, P. Zhang, W.S. Xia, Ceram. Int. **38**, 1391–1398 (2012)

16. G.H. Huang, D.X. Zhou, J.M. Xu, X.P. Chen, D.L. Zhang, W.Z. Lu, B.Y. Li, Mater. Sci. Eng.: B **99**, 416–420 (2003)
17. C.S. Liu, X.Q. Chen, P.C. Zhang, Q.Z. Wen, L.Z. Ma, H. Li, Ceram. Int. **49**, 95–100 (2023)
18. C.Z. Yin, C.C. Li, G.J. Yang, L. Fang, Y.H. Yuan, L.L. Shu, J. Khaliq, J. Eur. Ceram. Soc. **40**, 386–390 (2020)
19. J. Li, Y. Tang, Z.W. Zhang, W.S. Fang, L.Y. Ao, A.H. Yang, L.J. Liu, L. Fang, J. Eur. Ceram. Soc. **41**, 1317–1323 (2021)
20. Y. Xiong, H.Y. Xie, Z.G. Rao, L.J. Liu, Z.F. Wang, C.C. Li, J. Adv. Ceram. **10**, 1360–1370 (2021)
21. C.Z. Yin, Z.Z. Yu, L.L. Shu, L.J. Liu, Y. Chen, C.C. Li, J. Adv. Ceram. **10**, 108–119 (2020)
22. H.R. Tian, J.J. Zheng, L.T. Liu, H.T. Wu, H. Kimura, Y.Z. Lu, Z.X. Yue, J. Mater. Sci. Technol. **116**, 121–129 (2022)
23. X.H. Feng, R. Liu, X.L. Xu, Y.Y. Tong, S.J. Zhang, J.C. He, J.W. Xu, X.Z. Fang, X. Wang, Chin. J. Catal. **42**, 396–408 (2021)
24. K.A. Irshad, P. Ances, R. Rajitha, T.R. Ravindran, V. Srihari, S. Kalavathi, J. Alloys Compd. **822**, 153657 (2020)